

Transport and entanglement growth in long-range random Clifford circuits

Jonas Richter,^{1,*} Oliver Lunt,² and Arijeet Pal¹

¹*Department of Physics and Astronomy, University College London, Gower Street, London, WC1E 6BT, UK*

²*School of Physics and Astronomy, University of Birmingham, Birmingham, B15 2TT, UK*

(Dated: May 23, 2022)

Conservation laws and hydrodynamic transport can constrain entanglement dynamics in isolated quantum systems, manifest in a slowdown of higher Rényi entropies. Here, we introduce a class of long-range random Clifford circuits with U(1) symmetry, which act as minimal models for more generic quantum systems and provide an ideal framework to explore this phenomenon. Depending on the exponent α controlling the probability $\propto r^{-\alpha}$ of gates spanning a distance r , transport in such circuits varies from diffusive to superdiffusive and then to superballistic. We unveil that the different hydrodynamic regimes reflect themselves in the asymptotic entanglement growth according to $S(t) \propto t^{1/z}$, where z is the α -dependent dynamical transport exponent. We explain this finding in terms of the inhibited operator spreading in U(1)-symmetric Clifford circuits, where the emerging light cones are intimately related to the transport behavior and are significantly narrower compared to circuits without conservation law. For sufficiently small α , we show that the presence of hydrodynamic modes becomes irrelevant such that $S(t)$ behaves similarly in circuits with and without conservation law. Our work sheds light on the interplay of transport and entanglement and emphasizes the usefulness of constrained Clifford circuits to explore questions in quantum many-body dynamics.

Introduction.— Fundamental questions on the origin of hydrodynamic transport and the spreading of entanglement in isolated quantum systems have experienced a renaissance in recent years [1–3], with novel experiments being able to probe concepts such as chaos and quantum information scrambling [4–7]. While much progress has been made due to sophisticated numerical methods (see, e.g., [8–13]), ideas from quantum information provide a useful lens on the universal features of quantum dynamics far from equilibrium. In particular, suitable random-circuit models faithfully capture aspects of generic quantum systems [14–17], including the flexibility to describe settings with conservation laws and constraints [18, 19], as well as dual-unitary [20, 21], time-periodic [22, 23], or nonunitary dynamics [24, 25]. Moreover, random circuits are particularly attractive in the context of today’s noisy intermediate-scale quantum devices [26–28], where they found applications to achieve a quantum computational advantage [29] and to explore operator entanglement [30].

In case of chaotic quantum systems with short-ranged interactions, conservation laws, e.g., total magnetization, give rise to hydrodynamic modes that typically decay diffusively at long times [31–34], whereas entanglement is expected to grow ballistically [35]. Remarkably, recent work unveiled that this picture is incomplete and that transport and entanglement dynamics are intimately related with each other [36, 37] (see also [38–40]). Specifically, it was found that diffusive transport can constrain higher Rényi entropies to increase diffusively [36],

$$S_{n>1}(t) \propto \sqrt{t}, \quad \text{where } S_n = \log_2 \text{tr}[\rho_A^n]/(1-n), \quad (1)$$

with $\rho_A = \text{tr}_B |\psi(t)\rangle \langle \psi(t)|$ denoting the reduced density matrix for a bipartition into subsystems A and B , and $|\psi(t)\rangle$ is the time-evolved pure state of the system. This is in contrast to the von Neumann entropy

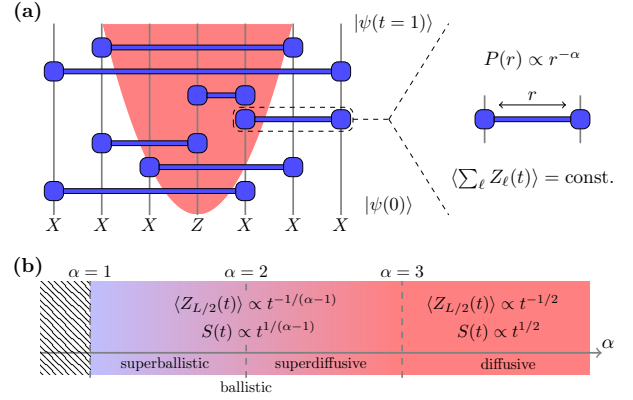


FIG. 1. (a) Two-qubit Clifford gates of range r occur with probability $P(r) \propto r^{-\alpha}$ and conserve the total Pauli-Z component [89], $\langle \psi(t) | \sum_{\ell} Z_{\ell} | \psi(t) \rangle = \text{const.}$ One time step for a $1d$ system of L qubits consists of L random gates. (b) By tuning $\alpha > 1$, different hydrodynamic regimes with dynamical exponent z [Eq. (2)] emerge, manifest in the tails of the circuit-averaged expectation value $\langle Z_{L/2}(t) \rangle \propto t^{-1/z}$ for initial state with single Z excitation in the center. Entanglement saturates approximately on a time scale $\propto L^z$, implying that it asymptotically mirrors the transport behavior, $S(t) \propto t^{1/z}$.

$S_1 = -\text{tr}[\rho_A \log_2 \rho_A]$, which was found to grow linearly as usual, $S_1(t) \propto t$. In this Letter, we demonstrate that this phenomenon of constrained entanglement dynamics occurs more generically also for transport types other than diffusion, and can be readily explored in a class of U(1)-symmetric random long-range Clifford circuits, see Fig. 1 (a). Depending on the exponent α that controls the probability $P(r) \propto r^{-\alpha}$ of gates spanning a distance r , the emerging transport behavior can be tuned from diffusive to superdiffusive and then to superballistic. Such circuits can be seen as minimal models to describe the

dynamics of long-range Hamiltonian systems with interactions decaying as $\propto r^{-\alpha'}$, with $\alpha' = \alpha/2$ [41, 42]. In particular, while Clifford gates are not sufficient for universal quantum computation, they form unitary 2-designs [43] (3-designs for qubits [44]), such that circuit averages of, e.g., entanglement growth or correlation functions, can be similar to more generic quantum evolutions [16].

Quantum systems with long-range interactions are ubiquitous in nature, including systems with dipolar or van der Waals interactions [45], with experimental realizations in a variety of platforms [46–51]. In contrast to short-range models, where Lieb-Robinson bounds confine correlations to a linear “light cone” [52], long-range interactions may lead to faster information propagation [53, 54]. Much effort has been invested to tighten Lieb-Robinson-like bounds for power-law interacting models [41, 55–65], as well as to study transport, correlation spreading, and entanglement dynamics [42, 66–74]. For chaotic systems in d dimensions, it was argued in [41, 62] that linear light cones arise for $\alpha' > d + 1/2$, where the properties become similar to those of short-range models, while power-law or logarithmic bounds emerge for $d/2 < \alpha' < d + 1/2$. For $\alpha' < d/2$, locality breaks down and information propagation becomes essentially instantaneous [75].

From a numerical point of view, long-range quantum systems are challenging due to quick entanglement generation and strong finite-size effects [76] (although entanglement can grow more slowly in some cases [70, 71]). In contrast, the class of random Clifford circuits considered in this Letter can be simulated efficiently even for large systems. Summarizing our main results, we unveil a direct correspondence between transport and entanglement growth, with entanglement saturating on a time scale $t_{\text{sat}} \propto L^z$ implying an asymptotic scaling $S(t) \propto t^{1/z}$, where z is the dynamical transport exponent, see Fig. 1 (b). We explain this finding in terms of the inhibited operator spreading in U(1)-symmetric Clifford circuits, leading to narrower light cones compared to circuits without conservation law. Moreover, we demonstrate that the constraint on $S(t)$ imposed by the conservation law becomes insignificant once transport becomes ballistic.

Clifford circuits with conservation law.— Clifford circuits are of major interest in quantum information [77], playing key roles in quantum error correction and randomized benchmarking [78, 79]. In the context of quantum many-body dynamics, Clifford circuits have recently gained popularity to study measurement-induced entanglement transitions (see e.g., [42, 80–84]). The main advantage is their efficient simulability on classical computers such that large system sizes can be accessed [85, 86]. The key idea is to exploit the stabilizer formalism [77, 87], where a quantum state $|\psi\rangle$ on L qubits can be uniquely defined by L operators \mathcal{O}_i , i.e., $\mathcal{O}_i |\psi\rangle = |\psi\rangle$, where $\mathcal{O}_i = X_1^{\nu_1^i} Z_1^{\mu_1^i} \dots X_L^{\nu_L^i} Z_L^{\mu_L^i}$ are L -site Pauli strings and $\nu_\ell^i, \mu_\ell^i = \{0, 1\}$, see [85]. Since Clifford gates preserve

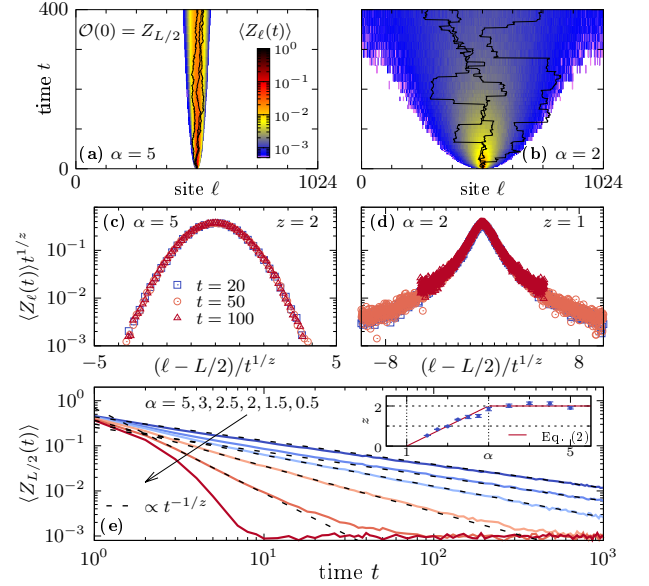


FIG. 2. [(a),(b)] $\langle Z_\ell(t) \rangle$ averaged over $\sim 10^5$ circuit realizations for $\alpha = 5$ and $\alpha = 2$ and $L = 1024$. Solid curves indicate results for individual circuit realizations, i.e., random-walks with step-size distribution $\propto r^{-\alpha}$. [(c),(d)] $\langle Z_\ell(t) \rangle t^{1/z}$ at fixed t , plotted against $(\ell - L/2)/t^{1/z}$. (e) $\langle Z_{L/2}(t) \rangle$ for different α (arrow). Dashed lines indicate power law $\propto t^{-1/z}$. Inset shows z extracted from the fits and compared to Eq. (2).

the Pauli group, the action $|\psi\rangle \rightarrow \mathcal{U}|\psi\rangle$ of a Clifford gate \mathcal{U} can be efficiently described by the stabilizers, $\mathcal{U}\mathcal{O}_i\mathcal{U}^\dagger$ [88], e.g., by storing the ν_ℓ^i, μ_ℓ^i in a binary matrix \mathcal{M} and updating their values appropriately [85].

In this Letter, we show that random Clifford circuits can elucidate the interplay between transport and entanglement growth [38]. We consider circuits with a U(1) symmetry, where one time step is defined as the application of L two-site gates conserving the total magnetization, $\langle \psi(t) | \sum_\ell Z_\ell | \psi(t) \rangle = \text{const.}$, cf. Fig. 1. This property is quite restrictive: While the full two-qubit Clifford group has 11520 distinct elements (modulo a global phase), generated by of phase, Hadamard, and controlled-not gates [85], only 64 conserve the total Pauli-Z component, see [89]. Moreover, due to the U(1) symmetry and the Pauli-preserving property of Clifford gates, it turns out that transport can be understood classically in terms of long-range random walks, so called Lévy flights. However, we will show that such constrained circuits still lead to extensive entanglement generation, thereby providing insights into more generic quantum systems.

Product states such as $|\rightarrow\rangle^{\otimes L}$ with spins pointing along the x direction can be stabilized by operators $\mathcal{O}_i = X_i$ ($i = 1, \dots, L$) that act nontrivially only on a single lattice site. Evolving $|\psi\rangle$ with respect to a random circuit will typically cause the \mathcal{O}_i to become more nonlocal, which results in increased entanglement. Clifford circuits are special, however, as they generate flat entanglement spec-

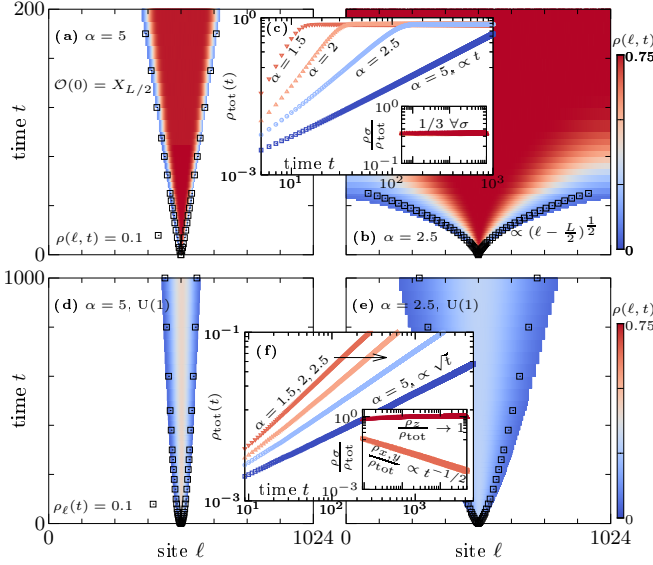


FIG. 3. [(a),(b)] Averaged $\rho(\ell, t)$ in full Clifford circuits with $\alpha = 5$ and $\alpha = 2.5$, obtained from $\mathcal{O}(0) = X_{L/2}$ with $L = 1024$. Symbols indicate $\rho(\ell, t) = 10^{-1}$. (c) $\rho_{\text{tot}}(t)$ for $L = 2048$ and different α (see also [89]). Inset shows $\rho_{\sigma}(t)/\rho_{\text{tot}}(t) \approx 1/3$, i.e., all Σ^{σ} contribute equally. Panels (d), (e) and (f) show analogous data, but for U(1)-symmetric circuits, where $\mathcal{O}(t)$ now spreads significantly slower. This stems from the dominant contribution of Z operators within $\rho_{\text{tot}}(t)$, cf. inset in (f) for $\alpha = 5$, where $\rho_z(t)/\rho_{\text{tot}}(t) \rightarrow 1$ while $\rho_{x,y}/\rho_{\text{tot}}(t) \propto t^{-1/2}$.

tra such that all S_n are equivalent [92]. While the different behaviors of S_1 and $S_{n>1}$ demonstrated in [36] therefore cannot be resolved, $S(t)$ is nevertheless sensitive to the presence of conservation laws and $S(t) \propto \sqrt{t}$ was found in Clifford circuits with diffusive transport [38]. Here, we show that circuits with long-range gates provide an ideal framework to study entanglement dynamics also for other transport types. To this end, let us reiterate the arguments of [36, 37] to explain the constrained entanglement growth: Consider the reduced density matrix ρ_A , which has χ nonzero eigenvalues $\Lambda_1 \leq \dots \leq \Lambda_{\chi}$. In the presence of hydrodynamic modes described by a dynamical exponent z , Λ_{χ} can be lower bounded by $\Lambda_{\chi} \gtrsim e^{-\gamma t^{1/z}}$ with some constant γ , where $z = 2$ corresponds to normal diffusion [36, 37]. This bound results from rare contributions to the state $|\psi(t)\rangle$, where qubits in a region of length ξ around the cut between A and B are all in the $|\uparrow\rangle$ state, acting as a bottleneck for entanglement generation as it takes time $\propto \xi^z$ for a $|\downarrow\rangle$ to get across the cut. It follows that $S_{n \rightarrow \infty} = -\log_2 \Lambda_{\chi}$ scales as $S_{\infty}(t) \propto t^{1/z}$ and, due to the inequality $S_{\infty} \leq S_{n>1} \leq n S_{\infty}/(n-1)$, all $S_{n>1}(t)$ obey this scaling. This argument does not depend on the type of time evolution and generalizes to U(1)-symmetric Clifford circuits, where $\Lambda_i = \Lambda$ and $S_n(t) \equiv S(t)$.

Hydrodynamics in long-range circuits.— By varying the exponent α , it is possible to tune the nature of transport in the random circuit. Consider an initial state $|\psi\rangle =$

$|\rightarrow\rangle^{\otimes L/2-1} |\uparrow\rangle |\rightarrow\rangle^{\otimes L/2}$, stabilized by X_{ℓ} for $\ell \neq L/2$, and Z_{ℓ} for $\ell = L/2$, cf. Fig. 1 (a). The action $\mathcal{U}\mathcal{O}_i\mathcal{U}^{\dagger}$ of the U(1)-symmetric Clifford gates on the two classes of stabilizers of $|\psi\rangle$ is quite different. Namely, while the $L-1$ stabilizers initialized with X_{ℓ} will become nonlocal and generate entanglement (discussed below), the stabilizer initialized with $Z_{L/2}$ will remain of length one throughout the entire circuit [89]. Specifically, the isolated Z operator will perform α -dependent long-range random walks, i.e., Lévy flights [93, 94], selected examples of which are shown in Figs. 2 (a) and (b) for $\alpha = 5$ and $\alpha = 2$. As a consequence, at a given time step, there will be a single site ℓ with $\langle\psi(t)|Z_{\ell}|\psi(t)\rangle = 1$, which is unentangled with the rest of the system [95]. This is in contrast to U(1)-symmetric Haar-random gates, where the Z excitation will be distributed over multiple sites.

Simulating 1d random circuits with $L = 1024$ (see [89] for 2d circuits), we further plot in Figs. 2 (a) and (b) the circuit-averaged value $\langle Z_{\ell}(t) \rangle$ for $\sim 10^5$ random realizations of $\mathcal{U}Z_{L/2}\mathcal{U}^{\dagger}$, highlighting that the circuit changes from local to non-local when reducing α . Analyzing $\langle Z_{\ell}(t) \rangle$ at fixed t , we find Gaussian profiles for $\alpha = 5$ that collapse when rescaled appropriately [cf. Fig. 2 (c)], indicating normal diffusion. In contrast, $\langle Z_{\ell}(t) \rangle$ is non-Gaussian for $\alpha = 2$ but rather described by a Lorentzian, signaling superdiffusive or ballistic transport [66, 67]. (See [89] for other α .) The α -dependent transport regimes are also reflected in the decay of the excitation at the central site, $\langle Z_{L/2}(t) \rangle \propto t^{-1/z}$, where z approximately follows the theoretical Lévy-flight prediction [67, 96], see Fig. 2 (e),

$$z = \begin{cases} 2, & \alpha \geq 3; \\ \alpha - 1, & 1 < \alpha \leq 3, \end{cases} \quad (2)$$

with no hydrodynamic tail for $\alpha \leq 1$. We attribute the residual differences between the extracted z values and Eq. (2) to finite system sizes and simulation times. Such finite-size effects are discussed in more detail in our analysis of entanglement growth, see Fig. 4 (d) and [89].

Operator spreading.— Before turning to entanglement, it is instructive to study the spreading of isolated operators. While we discussed in Fig. 2 that $\mathcal{U}Z_{\ell}\mathcal{U}^{\dagger}$ remains a single-site operator for U(1)-symmetric Clifford gates, we now consider $\mathcal{O} = X_{\ell}$. Generally, $\mathcal{O}(t) = \sum_{\mathcal{S}} \alpha_{\mathcal{S}}(t) \mathcal{S}$ can be expanded in the basis spanned by the 4^L Pauli strings \mathcal{S} . Evolution with respect to Haar-random gates increases the number of nonzero $\alpha_{\mathcal{S}}(t)$ [14–16], leading to operator entanglement [97]. Moreover, the strings \mathcal{S} on average involve a growing number of non-identity operators, known as operator spreading. In contrast, Clifford gates map Pauli operators on to each other, $\mathcal{O}(t) = \delta_{\mathcal{S}, \mathcal{O}(t)} \mathcal{S}$, and no operator entanglement is generated. However, $\mathcal{O}(t)$ will typically become nonlocal, manifested by its growing support $\rho_{\text{tot}}(t) = \frac{1}{L} \sum_{\ell, \sigma} \rho_{\sigma}(\ell, t)$, where $\rho_{\sigma}(\ell, t) = \text{tr}[\mathcal{O}_{\ell}(t) \Sigma^{\sigma}]/2$ and $\mathcal{O}_{\ell}(t)$ is the matrix at position ℓ in the string and $\Sigma^{\sigma} = \{X, Y, Z\}$, $\sigma = x, y, z$.

Considering $\mathcal{O}(0) = X_{L/2}$, we plot $\rho(\ell, t) = \sum_{\sigma} \rho_{\sigma}(\ell, t)$ in Fig. 3, which can be seen as a measure for the out-of-time-ordered correlator between operators at sites ℓ and $L/2$ [98]. The emerging light cones in Fig. 3 provide an upper bound for the dynamics of entanglement studied in Fig. 4. Several comments are in order. For circuits without conservation law [Figs. 3 (a),(b)], we observe a linear light cone for $\alpha = 5$, while a power-law light cone emerges for $\alpha = 2.5$, in agreement with the phase diagram for long-range systems obtained in [41]. Correspondingly, we find $\rho_{\text{tot}}(t) \propto t$ at $\alpha = 5$ and faster growth for smaller α [Fig. 3 (c)], see [89] for further details. Moreover, the bulk of the light cone is fully scrambled with $\rho(\ell, t) \rightarrow 3/4$ and $\rho_{\sigma}(t)/\rho_{\text{tot}}(t) \approx 1/3$ [insets in Fig. 3 (c)], where $\rho_{\sigma}(t) = \sum_{\ell} \rho_{\sigma}(\ell, t)$ is the Pauli-component resolved support. Next, turning to U(1)-symmetric gates, the behavior of $\rho(\ell, t)$ changes drastically [Figs. 3 (d),(e)]. Namely, operator spreading is significantly slower and is found to resemble the transport behavior of the conserved quantity [cf. Eq. (2)], with a diffusive (superdiffusive) light cone for $\alpha = 5$ ($\alpha = 2.5$), also reflected in the growth of $\rho_{\text{tot}}(t)$ [Fig. 3 (f)]. This can be understood due to the inhomogeneous composition of the operator string $\mathcal{O}(t)$ in U(1)-symmetric circuits: Focusing on $\alpha = 5$, we find $\rho_z(t) \propto t^{1/2}$, while $\rho_{x,y}(t) = \text{const.}$, such that $\rho_{x,y}(t)/\rho_{\text{tot}}(t) \propto t^{-1/2}$ and $\rho_z(t)/\rho_{\text{tot}}(t) \rightarrow 1$ [inset in Fig. 3 (f)]. Thus, due to the U(1)-symmetric gates, $\mathcal{O}(t)$ will be dominated by conserved Z operators [89] which spread as in Fig. 2, leading to narrower light cones and constrained entanglement dynamics. We note that this appears to be in contrast to Haar-random circuits with conservation law, where the front of the light cone is dominated by the nonconserved operators [18].

Entanglement growth.— We now discuss entanglement dynamics in long-range Clifford circuits. Choosing the initial state $|\psi\rangle = |\rightarrow\rangle^{\otimes L}$, stabilized by X_{ℓ} everywhere, we calculate $S(t) = \text{rank}(\mathcal{M}_{L/2}) - L/2$ for a half-system bipartition, where $\mathcal{M}_{L/2}$ denotes the stabilizer matrix restricted to the first $L/2$ sites [14, 99, 100]. From this expression, it is clear that $S(t)$ depends on the collective dynamics of all L stabilizers of $|\psi(t)\rangle$. We thus expect that the spreading of individual X_{ℓ} discussed in Fig. 3 provides an upper bound for the growth of $S(t)$ [14].

Since $|\psi\rangle$ is a superposition of all symmetry sectors, $S(t \rightarrow \infty) \approx L/2$ saturates at the same value in circuits with and without the conservation law, cf. Figs. 4 (a) and (b). We find it convenient to analyze the α -dependence of $S(t)$ by extracting the saturation time $t_{\text{sat}} \propto L^z$ for different L , implying an asymptotic scaling $S(t) \propto t^{1/z}$. Fig. 4 (c) shows some examples of this scaling for U(1)-symmetric circuits. The obtained values of z are summarized in Fig. 4 (e). In the case of U(1)-symmetric circuits, we find that the different hydrodynamic regimes are reflected in the entanglement dynamics and z is indeed reasonably well described by Eq. (2). Furthermore, while we recover $z \rightarrow 1$ in unsymmetric circuits for $\alpha \geq 3$,

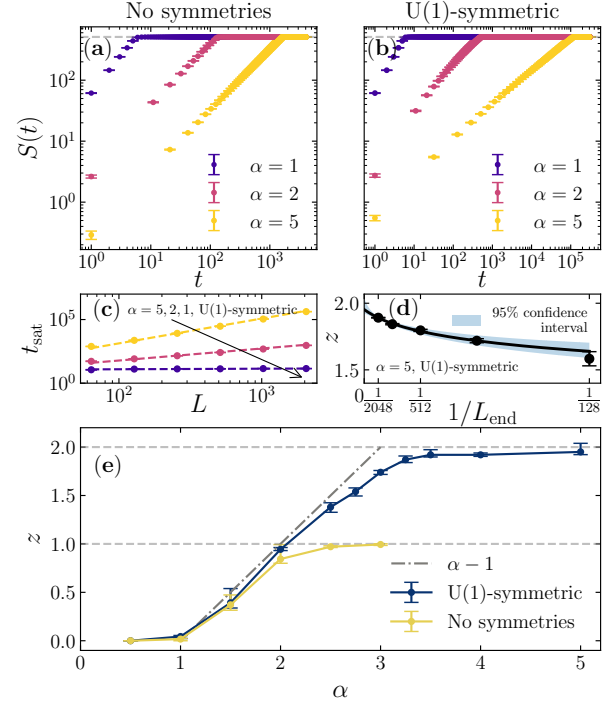


FIG. 4. [(a),(b)] $S(t)$ for different α in asymmetric and U(1)-symmetric circuits with $L = 1024$ and open boundaries. For $\alpha \geq 3$, we expect short-range behavior: $z = 2$ with U(1) symmetry and $z = 1$ without. (c) Scaling of the saturation time t_{sat} vs L . The dashed lines are power-law fits $t_{\text{sat}} \sim L^z$, with z extracted from the extrapolation procedure. (d) An example of the extrapolation procedure we use to estimate finite-size effects for z , see [89]. (e) z versus α for circuits with and without conservation law. For $\alpha \lesssim 2$, transport becomes (super)ballistic and entanglement dynamics becomes similar for both gate sets. The deviations from Eq. (2) around $\alpha = 3$ may be due to logarithmic corrections to transport [67].

as expected for short-range models [14], we observe that the scaling behaviors of circuits with and without conservation law become very similar for $\alpha \lesssim 2$, with all discrepancies in z estimates contained within error bars. This can be understood from the fact that once α is sufficiently small, transport becomes ballistic or superballistic [cf. Fig. 1 (b)], such that the constraint imposed by the conservation law becomes insignificant. Eventually, for $\alpha \leq 1$, $S(t)$ saturates in $\mathcal{O}(1)$ time and $z \rightarrow 0$.

Let us comment on the residual deviations of the extracted z values in Fig. 4 (e) from the prediction (2), most pronounced near $\alpha = 3$ where transport crosses over from short-range to long-range. These deviations may partly be due to significant finite-size effects. In fact, even at the large system sizes $L \sim 10^3$ presented here, we observe a drift of z with increasing L . We attempt to account for this in our analysis by performing a $1/L$ extrapolation: For a range of system sizes L_{end} , we artificially restrict our data set to $L \leq L_{\text{end}}$ and extract an estimate $z(L_{\text{end}})$. We then fit these estimates to a power law in $1/L_{\text{end}}$

and extrapolate to the $1/L_{\text{end}} \rightarrow 0$ limit, as exemplified in Fig. 4 (d). For details, including how we obtain the error bars using a Monte-Carlo scheme, see [89]. Precisely at $\alpha = 3$, it is known from the theory of Lévy flights that transport can receive logarithmic corrections [67], which may explain the faster than expected entanglement growth. Indeed, if we repeat our analysis, but with the ansatz $S(t) \sim t^{1/z} \sqrt{\log t}$, we obtain $z = 1.91(1)$ much closer to the expected $z = 2$ [101]. The marginality at $\alpha \approx 3$ is also reflected in the development of heavy non-Gaussian tails in both $\langle Z_\ell(t) \rangle$ and $\rho(\ell, t)$, see [89].

Conclusions and Outlook.— To summarize, we have studied the interplay of transport and entanglement dynamics in long-range random Clifford circuits with U(1) conservation law. As a main result, we demonstrated that the emerging transport regimes with dynamical exponent z reflect themselves in the growth of entanglement as $S(t) \propto t^{1/z}$, which generalizes earlier work that has focused on diffusive systems with $z = 2$ [36]. We have argued that this can be understood due to the inhibited operator spreading in U(1)-symmetric Clifford circuits, where operator strings become dominated by the conserved quantity. While this picture may not directly apply to other settings (e.g., Haar-random gates with conservation law), we expect our findings for $S(t)$ to hold also in more generic quantum many-body systems.

A promising direction of research is to consider entanglement dynamics in efficiently simulable Clifford circuits with other gate sets or conservation laws, potentially giving rise to localized transport behavior [102], as well as adding projective measurements which can induce various nonequilibrium phases in circuits with symmetry [103, 104]. In this context, studying the impact of sporadic non-Clifford gates, which can act as seeds of chaos [105], is another natural avenue. Finally, it would be interesting if the transport-dependent growth of higher Rényi entropies can be observed experimentally with analog quantum simulators or noisy intermediate-scale quantum computers, where diffusive or superdiffusive transport can be emulated [106, 107] and the pertinent Rényi-2 entropy is accessible at least for small system sizes [108, 109].

Acknowledgments.— We sincerely thank Lluís Masanes for a helpful comment. This work was funded by the European Research Council (ERC) under the European Union’s Horizon 2020 research and innovation programme (Grant agreement No. 853368). O.L. acknowledges support by UK Research and Innovation (UKRI) [grant number MR/T040947/1].

* j.richter@ucl.ac.uk

- [1] L. D’Alessio, Y. Kafri, A. Polkovnikov, and M. Rigol, *Adv. Phys.* **65**, 239 (2016).
- [2] R. Nandkishore and D. A. Huse, *Annu. Rev. Condens. Matter Phys.* **6**, 15 (2015).

- [3] B. Bertini, F. Heidrich-Meisner, C. Karrasch, T. Prosen, R. Steinigeweg, and M. Žnidarič, *Rev. Mod. Phys.* **93**, 025003 (2021).
- [4] J. Li, R. Fan, H. Wang, B. Ye, B. Zeng, H. Zhai, X. Peng, and J. Du, *Phys. Rev. X* **7**, 031011 (2017).
- [5] M. Gärttner, J. G. Bohnet, A. Safavi-Naini, M. L. Wall, J. J. Bollinger, and A. M. Rey, *Nat. Phys.* **13**, 781 (2017).
- [6] K. A. Landsman, C. Figgatt, T. Schuster, N. M. Linke, B. Yoshida, N. Y. Yao, and C. Monroe, *Nature* **567**, 61 (2019).
- [7] M. S. Blok, V. V. Ramasesh, T. Schuster, K. O’Brien, J. M. Kreikebaum, D. Dahlen, A. Morvan, B. Yoshida, N. Y. Yao, and I. Siddiqi, *Phys. Rev. X* **11**, 021010 (2021).
- [8] J. Haegeman, J. I. Cirac, T. J. Osborne, I. Pižorn, H. Verschelde, and F. Verstraete, *Phys. Rev. Lett.* **107**, 070601 (2011).
- [9] S. Paeckel, T. Köhler, A. Swoboda, S. R. Manmana, U. Schollwöck, and C. Hubig, *Ann. Phys.* **411**, 167998 (2019).
- [10] T. Rakovszky, C. W. von Keyserlingk, and F. Pollmann, *Phys. Rev. B* **105**, 075131 (2022).
- [11] C. D. White, M. Zaletel, R. S. K. Mong, and G. Refael, *Phys. Rev. B* **97**, 035127 (2018).
- [12] J. Wurtz, A. Polkovnikov, and D. Sels, *Ann. Phys.* **395**, 341 (2018).
- [13] T. Heitmann, J. Richter, D. Schubert, and R. Steinigeweg, *Z. Naturforsch. A* **75**, 421 (2020).
- [14] A. Nahum, J. Ruhman, S. Vijay, and J. Haah, *Phys. Rev. X* **7**, 031016 (2017).
- [15] C. W. von Keyserlingk, T. Rakovszky, F. Pollmann, and S. L. Sondhi, *Phys. Rev. X* **8**, 021013 (2018).
- [16] A. Nahum, S. Vijay, and J. Haah, *Phys. Rev. X* **8**, 021014 (2018).
- [17] F. G. S. L. Brandão, W. Chemissany, N. Hunter-Jones, R. Kueng, and J. Preskill, *PRX Quantum* **2**, 030316 (2021).
- [18] V. Khemani, A. Vishwanath, and D. A. Huse, *Phys. Rev. X* **8**, 031057 (2018).
- [19] S. Moudgalya, A. Prem, D. A. Huse, and A. Chan, *Phys. Rev. Research* **3**, 023176 (2021).
- [20] B. Bertini, P. Kos, and T. Prosen, *Phys. Rev. Lett.* **123**, 210601 (2019).
- [21] P. W. Claeys and A. Lamacraft, *Phys. Rev. Lett.* **126**, 100603 (2021).
- [22] B. Bertini, P. Kos, and T. Prosen, *Phys. Rev. Lett.* **121**, 264101 (2018).
- [23] A. Chan, A. De Luca, and J. T. Chalker, *Phys. Rev. Lett.* **121**, 060601 (2018).
- [24] B. Skinner, J. Ruhmann, and A. Nahum, *Phys. Rev. X* **9**, 031009 (2019).
- [25] A. C. Potter and R. Vasseur, *arXiv:2111.08018*.
- [26] J. Preskill, *Quantum* **2**, 79 (2018).
- [27] J. Richter and A. Pal, *Phys. Rev. Lett.* **126**, 230501 (2021).
- [28] O. Lunt, J. Richter, and A. Pal, *arXiv:2112.06682*.
- [29] F. Arute *et al.*, *Nature* **574**, 505 (2019).
- [30] X. Mi *et al.*, *Science* **374**, 1479 (2021).
- [31] J. Lux, J. Müller, A. Mitra, and A. Rosch, *Phys. Rev. A* **89**, 053608 (2014).
- [32] A. Bohrdt, C. B. Mendl, M. Endres, and M. Knap, *New J. Phys.* **19**, 063001 (2017).
- [33] J. Richter, F. Jin, H. De Raedt, K. Michielsen, J. Gemmer, and R. Steinigeweg, *Phys. Rev. B* **97**, 174430 (2018).
- [34] J. Richter, F. Jin, L. Knipschild, J. Herbrych, H. De Raedt, K. Michielsen, J. Gemmer, and R. Steinigeweg, *Phys. Rev. B* **98**, 144422 (2019).

- [35] H. Kim and D. A. Huse, Phys. Rev. Lett. **111**, 127205 (2013).
- [36] T. Rakovszky, F. Pollmann, and C. W. von Keyserlingk, Phys. Rev. Lett. **122**, 250602 (2019).
- [37] Y. Huang, IOP SciNotes **1**, 035205 (2020).
- [38] M. Žnidarič, Commun. Phys. **3**, 100 (2020).
- [39] T. Rakovszky, F. Pollmann, and C. von Keyserlingk, Commun. Phys. **4**, 91 (2021).
- [40] T. Zhou and A. W. W. Ludwig, Phys. Rev. Research **2**, 033020 (2020).
- [41] T. Zhou, S. Xu, X. Chen, A. Guo, and B. Swingle, Phys. Rev. Lett. **124**, 180601 (2020).
- [42] M. Block, Y. Bao, S. Choi, E. Altman, and N. Y. Yao, Phys. Rev. Lett. **128**, 010604 (2022).
- [43] A. W. Harrow and R. A. Low, Comm. Math. Phys. **291**, 257 (2009).
- [44] Z. Webb, Quantum Inf. Comput. **16**, 1379 (2016).
- [45] M. Saffman, T. G. Walker, K. Mølmer, Rev. Mod. Phys. **82**, 2313 (2010).
- [46] D. Porras and J. I. Cirac, Phys. Rev. Lett. **92**, 207901 (2004).
- [47] P. Jurcevic, B. P. Lanyon, P. Hauke, C. Hempel, P. Zoller, R. Blatt, and C. F. Roos, Nature (London) **511**, 202 (2014).
- [48] J. Smith, A. Lee, P. Richerme, B. Neyenhuis, P. W. Hess, P. Hauke, M. Heyl, D. A. Huse, and C. Monroe, Nat. Phys. **12**, 907 (2016).
- [49] P. Richerme, Z.-X. Gong, A. Lee, C. Senko, J. Smith, M. Foss-Feig, S. Michalakakis, A. V. Gorshkov, and C. Monroe, Nature (London) **511**, 198 (2014).
- [50] H. Bernien, S. Schwartz, A. Keesling, H. Levine, A. Omran, H. Pichler, S. Choi, A. S. Zibrov, M. Endres, M. Greiner, V. Vuletić, and M. D. Lukin, Nature **551**, 579 (2017).
- [51] A. Periwal, E. S. Cooper, P. Kunkel, J. F. Wienand, E. J. Davis, and M. Schleier-Smith, Nature **600**, 630 (2021).
- [52] E. H. Lieb and D. W. Robinson, Commun. Math. Phys. **28**, 251 (1972).
- [53] N. Lashkari, D. Stanford, M. Hastings, T. Osborne, and P. Hayden, J. High Energy Phys. **2013**, 22 (2013).
- [54] M. Avellino, A. J. Fisher, and S. Bose, Phys. Rev. A **74**, 012321 (2006).
- [55] M. B. Hastings and T. Koma, Commun. Math. Phys. **265**, 781 (2006).
- [56] J. Eisert, M. van den Worm, S. R. Manmana, and M. Kastner, Phys. Rev. Lett. **111**, 260401 (2013).
- [57] P. Hauke and L. Tagliacozzo, Phys. Rev. Lett. **111**, 207202 (2013).
- [58] M. Foss-Feig, Z.-X. Gong, C. W. Clark, and A. V. Gorshkov, Phys. Rev. Lett. **114**, 157201 (2015).
- [59] M. C. Tran, A. Y. Guo, Y. Su, J. R. Garrison, Z. Eldredge, M. Foss-Feig, A. M. Childs, and A. V. Gorshkov, Phys. Rev. X **9**, 031006 (2019).
- [60] D. J. Luitz and Y. Bar Lev, Phys. Rev. A **99**, 010105(R) (2019).
- [61] L. Colmenarez and D. J. Luitz, Phys. Rev. Research **2**, 043047 (2020).
- [62] T. Zhou and X. Chen, Phys. Rev. E **99**, 052212 (2019).
- [63] T. Kuwahara and K. Saito, Phys. Rev. X **10**, 031010 (2020).
- [64] M. C. Tran, A. Y. Guo, C. L. Baldwin, A. Ehrenberg, A. V. Gorshkov, and A. Lucas, Phys. Rev. Lett. **127**, 160401 (2021).
- [65] C.-F. Chen and A. Lucas, Phys. Rev. A **104**, 062420 (2021).
- [66] B. Kloss and Y. Bar Lev, Phys. Rev. A **99**, 032114 (2019).
- [67] A. Schuckert, I. Lovas, and M. Knap, Phys. Rev. B **101**, 020416 (2020).
- [68] L. Cevolani, G. Carleo, and L. Sanchez-Palencia, New J. Phys. **18**, 093002 (2016).
- [69] T. Hashizume, S. Kuriyattil, A. J. Daley, and G. Bentsen, arXiv:2202.11750.
- [70] J. Schachenmayer, B. P. Lanyon, C. F. Roos, and A. J. Daley, Phys. Rev. X **3**, 031015 (2013).
- [71] S. Pappalardi, A. Russomanno, B. Žunkovič, F. Iemini, A. Silva, and R. Fazio, Phys. Rev. B **98**, 134303 (2018).
- [72] T. Kuwahara and K. Saito, Phys. Rev. Lett. **126**, 030604 (2021).
- [73] T. Minato, K. Sugimoto, T. Kuwahara, and K. Saito, Phys. Rev. Lett. **128**, 010603 (2022).
- [74] T. Müller, S. Diehl, and M. Buchhold, Phys. Rev. Lett. **128**, 010605 (2022).
- [75] R. Bachelard and M. Kastner, Phys. Rev. Lett. **110**, 170603 (2013).
- [76] M. P. Zaletel, R. S. K. Mong, C. Karrasch, J. E. Moore, and F. Pollmann, Phys. Rev. B **91**, 165112 (2015).
- [77] M. A. Nielsen and I. L. Chuang, *Quantum Computation and Quantum Information* (Cambridge University Press, Cambridge, 2000).
- [78] E. Knill, D. Leibfried, R. Reichle, J. Britton, R. B. Blakestad, J. D. Jost, C. Langer, R. Ozeri, S. Seidelin, and D. J. Wineland, Phys. Rev. A **77**, 012307 (2008).
- [79] E. Magesan, J. M. Gambetta, and J. Emerson, Phys. Rev. Lett. **106**, 180504 (2011).
- [80] Y. Li, X. Chen, and M. P. A. Fisher, Phys. Rev. B **98**, 205136 (2018).
- [81] M. J. Gullans and D. A. Huse, Phys. Rev. X **10**, 041020 (2020).
- [82] S. Sharma, X. Turkeshi, R. Fazio, and M. Dalmonte, SciPost Phys. Core **5**, 023 (2022).
- [83] A. Lavasani, Y. Alavirad, and M. Barkeshli, Nat. Phys. **17**, 342 (2021).
- [84] O. Lunt, M. Szyniszewski, and A. Pal, Phys. Rev. B **104**, 155111 (2021).
- [85] S. Aaronson and D. Gottesman, Phys. Rev. A **70**, 052328 (2004).
- [86] S. Anders and H. J. Briegel, Phys. Rev. A **73**, 022334 (2006).
- [87] D. Gottesman, arXiv:quant-ph/9807006
- [88] Note that this expression differs from the usual Heisenberg picture, where the order of \mathcal{U} and \mathcal{U}^\dagger is reversed.
- [89] See supplemental material for details on the structure of the Clifford group, additional numerical results on transport, operator spreading, and entanglement dynamics in circuits with and without $U(1)$ symmetry, as well as in two-dimensional circuits, including Refs. [90, 91].
- [90] A. D. Córcoles, J. M. Gambetta, J. M. Chow, J. A. Smolin, M. Ware, J. D. Strand, B. L. T. Plourde, and M. Steffen, Phys. Rev. A **87**, 030301(R) (2013).
- [91] R. Koenig and J. A. Smolin, J. Math. Phys. **55**, 122202 (2014).
- [92] D. Fattal, T. S. Cubitt, Y. Yamamoto, S. Bravyi, and I. L. Chuang, arXiv:quant-ph/0406168.
- [93] R. Metzler and J. Klafter, Phys. Rep. **339**, 1 (2000).
- [94] V. Zaburdaev, S. Denisov, and J. Klafter, Rev. Mod. Phys. **87**, 483 (2015).
- [95] Note that if one were to simulate the dynamics of a state stabilized by $\pm Z_\ell$ on all lattice sites, i.e., a product state $|\uparrow\downarrow\cdots\rangle$ in the Z basis, evolution with respect to Z

conserving Clifford gates would be entirely classical with $S(t) = 0$ for all t . This is in contrast to Haar-random gates with $U(1)$ symmetry.

- [96] We emphasize again that this corresponds to $1d$ Hamiltonian systems with couplings $J \propto r^{-\alpha'}$, with $\alpha' = \alpha/2$.
- [97] P. Zanardi, Phys. Rev. A **63**, 040304(R) (2001).
- [98] S. Xu and B. Swingle, arXiv:2202.07060.
- [99] A. Hamma, R. Ionicioiu, and P. Zanardi, Phys. Rev. A **71**, 022315 (2005).
- [100] Note that the rank has to be calculated by treating the entries ν_ℓ^i, μ_ℓ^i of \mathcal{M} as elements of the field \mathbb{F}_2 , i.e., addition and multiplication are performed modulo 2.
- [101] In fact, we find the closest agreement with $z = 2$ if we make the ansatz $S(t) \sim t^{1/z} (\log t)^{2/3}$, from which we obtain $z = 1.98(1)$.
- [102] A. Chandran and C. R. Laumann, Phys. Rev. B **92**, 024301 (2015).
- [103] U. Agrawal, A. Zabalo, K. Chen, J. H. Wilson, A. C. Potter, J. H. Pixley, S. Gopalakrishnan, and R. Vasseur, arXiv:2107.10279.
- [104] Y. Bao, S. Choi, and E. Altman, Ann. Phys. **435**, 168618 (2021).
- [105] S. Zhou, Z. Yang, A. Hamma, and C. Chamon, SciPost Phys. **9**, 087 (2020).
- [106] M. K. Joshi, F. Kranzl, A. Schuckert, I. Lovas, C. Maier, R. Blatt, M. Knap, and C. F. Roos, Science **376**, 720 (2022).
- [107] D. Wei, A. Rubio-Abadal, B. Ye, F. Machado, J. Kemp, K. Srakaew, S. Hollerith, J. Rui, S. Gopalakrishnan, N. Y. Yao, I. Bloch, and J. Zeiher, Science **376**, 716 (2022).
- [108] R. Islam, R. Ma, P. M. Preiss, M. Eric Tai, A. Lukin, M. Rispoli, and M. Greiner, Nature **528**, 77 (2015).
- [109] N. M. Linke, S. Johri, C. Figgatt, K. A. Landsman, A. Y. Matsuura, and C. Monroe, Phys. Rev. A **98**, 052334 (2018).

SUPPLEMENTAL MATERIAL

Structure of the Clifford group

Let us provide additional explanations on random Clifford circuits. To begin with, we note that the Pauli group \mathcal{P}_L on L qubits is generated by L -fold tensor products of the Pauli matrices,

$$I = \begin{pmatrix} 1 & 0 \\ 0 & 1 \end{pmatrix}, \quad X = \begin{pmatrix} 0 & 1 \\ 1 & 0 \end{pmatrix}, \quad Y = \begin{pmatrix} 0 & -i \\ i & 0 \end{pmatrix}, \quad Z = \begin{pmatrix} 1 & 0 \\ 0 & -1 \end{pmatrix}. \quad (\text{S1})$$

The Clifford group \mathcal{C}_L on L qubits is then defined as the group that preserves the Pauli group \mathcal{P}_L under conjugation, quotiented by $U(1)$ to account for a global phase.

Clifford group on 2 qubits

The two-qubit Clifford group \mathcal{C}_2 can be generated by the gates $\{P, H, \text{CNOT}_{0,1}\}$, where

$$P = \begin{pmatrix} 1 & 0 \\ 0 & i \end{pmatrix}, \quad H = \begin{pmatrix} 1 & 1 \\ 1 & -1 \end{pmatrix}, \quad \text{CNOT}_{0,1} = \begin{pmatrix} 1 & 0 & 0 & 0 \\ 0 & 1 & 0 & 0 \\ 0 & 0 & 0 & 1 \\ 0 & 0 & 1 & 0 \end{pmatrix}, \quad \text{CNOT}_{1,0} = \begin{pmatrix} 1 & 0 & 0 & 0 \\ 0 & 0 & 0 & 1 \\ 0 & 0 & 1 & 0 \\ 0 & 1 & 0 & 0 \end{pmatrix}. \quad (\text{S2})$$

For convenience we further define the composite gates W and V ,

$$W = H \cdot P, \quad V = W \cdot W = H \cdot P \cdot H \cdot P. \quad (\text{S3})$$

The two-qubit Clifford group can then be structured into different classes, characterized by their number of two-qubit gates [S1]. The first class contains solely single-qubit gates,

$$(h_0 \otimes h_1)(v_0 \otimes v_1)(p_0 \otimes p_1), \quad \text{with } h_i \in \{I, H\}, \quad v_i \in \{I, V, W\} \text{ and } p_i \in \{I, X, Y, Z\}, \quad (\text{S4})$$

which results in $2^2 \times 3^2 \times 4^2 = 24^2 = 576$ distinct gates. The second class requires one CNOT gate,

$$(h_0 \otimes h_1)(v_0 \otimes v_1)\text{CNOT}_{0,1}(v'_0 \otimes v'_1)(p_0 \otimes p_1), \quad \text{with } h_i \in \{I, H\}, \quad v_i, v'_i \in \{I, V, W\}, \quad p_i \in \{I, X, Y, Z\}, \quad (\text{S5})$$

which contains $2^2 \times 3^2 \times 3^2 \times 4^2 = 5184$ gates. The third class comprises sequences with two CNOT gates,

$$(h_0 \otimes h_1)(v_0 \otimes v_1)\text{CNOT}_{0,1}\text{CNOT}_{1,0}(v'_0 \otimes v'_1)(p_0 \otimes p_1), \quad \text{with } h_i \in \{I, H\}, \quad v_i, v'_i \in \{I, V, W\}, \quad p_i \in \{I, X, Y, Z\}, \quad (\text{S6})$$

which yields $2^2 \times 3^2 \times 3^2 \times 4^2 = 5184$ gates. Eventually, the fourth class requires three CNOT gates,

$$(h_0 \otimes h_1)(v_0 \otimes v_1)\text{CNOT}_{0,1}\text{CNOT}_{1,0}\text{CNOT}_{0,1}(p_0 \otimes p_1), \quad \text{with } h_i \in \{I, H\}, \quad v_i \in \{I, V, W\}, \quad p_i \in \{I, X, Y, Z\}, \quad (\text{S7})$$

which contains $2^2 \times 3^2 \times 4^2 = 576$ gates. In total, there are thus 11520 distinct 2-qubit Clifford gates.

In practice, these 11520 distinct gates can be stored in a look-up table. Every application of a two-qubit Clifford gate in the circuit then corresponds to selecting and carrying out a random element of the look-up table. Alternatively, another useful approach to randomly select an element of \mathcal{C}_2 has been presented in [S2]. In essence, it consists of generating a suitable symplectic matrix, which upon multiplication with the stabilizer tableau, implements the action of a random gate. This approach is particularly beneficial if one is interested in Clifford gates on more than two qubits since $|\mathcal{C}_{n>2}|$ is too large to be stored in a look-up table. In this paper, we use both approaches complementarily.

2-qubit Clifford gates that conserve $\langle \psi(t) | Z_1 + Z_2 | \psi(t) \rangle$

In this paper, we are mainly interested in the interplay between transport and entanglement growth. To this end, we consider circuits with $U(1)$ symmetry that conserve the total Pauli- Z component, such that magnetization exhibits hydrodynamic transport. Given the decomposition of the full two-qubit Clifford group in Eqs. (S4) - (S7), the Clifford gates that conserve magnetization can be written as follows. The first class consists of single-qubit gates,

$$(h_0 \otimes h_1)(p_0 \otimes p_1), \quad \text{with } h_i \in \{I, P\}, \text{ and } p_i \in \{I, Z\}, \quad (\text{S8})$$

and contains $2^2 \times 2^2 = 4^2 = 16$ distinct gates. The second class requires one CNOT gates,

$$(h_0 \otimes h_1) \text{CNOT}_{0,1}(I \otimes W)(p_0 \otimes p_1), \text{ with } h_0 \in \{I, P\}, h_1 \in \{V, H\}, p_i \in \{I, Z\}, \quad (\text{S9})$$

and contains $2 \times 2 \times 2^2 = 16$ distinct gates. The third class requires two CNOT gates,

$$(h_0 \otimes h_1) \text{CNOT}_{0,1} \text{CNOT}_{1,0}(I \otimes W)(p_0 \otimes p_1), \text{ with } h_0 \in \{H, V\}, h_1 \in \{I, P\}, p_i \in \{I, Z\}, \quad (\text{S10})$$

and contains $2 \times 2 \times 2^2 = 16$ gates. Finally, the fourth class requires three CNOT gates,

$$(h_0 \otimes h_1) \text{CNOT}_{0,1} \text{CNOT}_{1,0} \text{CNOT}_{0,1}(p_0 \otimes p_1), \text{ with } h_i \in \{I, P\}, p_i \in \{I, Z\}, \quad (\text{S11})$$

and contains $2^2 \times 2^2 = 16$ gates. Thus, there are 64 distinct 2-qubit Clifford gates which conserve the magnetization $\langle \psi(t) | Z_1 + Z_2 | \psi(t) \rangle$. We note that this is distinctly smaller than the size of the full two-qubit Clifford group, $64 \ll |\mathcal{C}_2| = 11520$. Moreover, regarding the production of entanglement, let us note that in the full two-qubit Clifford group only 576 gates are separable [Eq. (S4)], which corresponds to a fraction of $576/11520 = 0.05$. In contrast, in the case of gates that conserve magnetization, $16/64 = 0.25$ gates are separable [Eq. (S8)]. Thus, if one considers Clifford circuits with U(1) symmetry, the application of a random gate will, on average, produce less entanglement compared to Clifford circuits without conservation law. This has the effect that, even in regimes where the dynamical critical exponent is the same for symmetric and asymmetric circuits, symmetric circuits will typically take longer (by some $\mathcal{O}(1)$ factor) to reach the steady-state value than asymmetric circuits.

It is also instructive to study the action of the U(1)-symmetric Clifford gates in Eqs. (S8) - (S11) on Pauli operators, $\mathcal{U}(\mathcal{O}_1 \otimes \mathcal{O}_2) \mathcal{U}^\dagger$. Given two lattice sites, as well as the Pauli and identity operators in Eq. (S1), there are 2^4 different configurations to consider. First of all, it is obvious that with probability $p = 1$,

$$I \otimes I \longrightarrow I \otimes I \quad (p = 1), \quad (\text{S12})$$

i.e., given identity operators on both lattice sites, this configuration remains unchanged for all 64 possible U(1)-symmetric Clifford gates. This result naturally holds for Clifford gates without conservation law as well. Crucially, for other nontrivial initial operator configurations, the effect of the U(1) conservation law becomes apparent. In particular, we have,

$$\left. \begin{array}{l} Z \otimes \mathbb{1} \\ \mathbb{1} \otimes Z \end{array} \right\} \longrightarrow \left\{ \begin{array}{l} Z \otimes \mathbb{1} \quad (p = 1/2) \\ \mathbb{1} \otimes Z \quad (p = 1/2) \end{array} \right\}, \quad Z \otimes Z \longrightarrow Z \otimes Z \quad (p = 1), \quad (\text{S13})$$

which highlights the fact that a single Z operator can perform jumps between different lattice sites, but no other operators are created in the process. As a consequence, if one starts with an isolated Z operator, the application of U(1)-symmetric Clifford gates will lead to a random-walk of the Z operator, but the operator string will remain of length one throughout the entire circuits.

In contrast, if the initial configuration contains solely X or Y operators, the U(1)-symmetric Clifford gates cannot produce new Z operators,

$$\left. \begin{array}{l} X \otimes X \\ Y \otimes Y \\ X \otimes Y \\ Y \otimes X \end{array} \right\} \longrightarrow \left\{ \begin{array}{ll} X \otimes X & (p = 1/4) \\ Y \otimes Y & (p = 1/4) \\ X \otimes Y & (p = 1/4) \\ Y \otimes X & (p = 1/4) \end{array} \right\}. \quad (\text{S14})$$

Finally, the remaining 8 configurations transform according to,

$$\left. \begin{array}{l} X \otimes \mathbb{1} \\ \mathbb{1} \otimes X \\ Y \otimes \mathbb{1} \\ \mathbb{1} \otimes Y \\ X \otimes Z \\ Z \otimes X \\ Y \otimes Z \\ Z \otimes Y \end{array} \right\} \longrightarrow \left\{ \begin{array}{ll} X \otimes \mathbb{1} & (p = 1/8) \\ \mathbb{1} \otimes X & (p = 1/8) \\ Y \otimes \mathbb{1} & (p = 1/8) \\ \mathbb{1} \otimes Y & (p = 1/8) \\ X \otimes Z & (p = 1/8) \\ Z \otimes X & (p = 1/8) \\ Y \otimes Z & (p = 1/8) \\ Z \otimes Y & (p = 1/8) \end{array} \right\}. \quad (\text{S15})$$

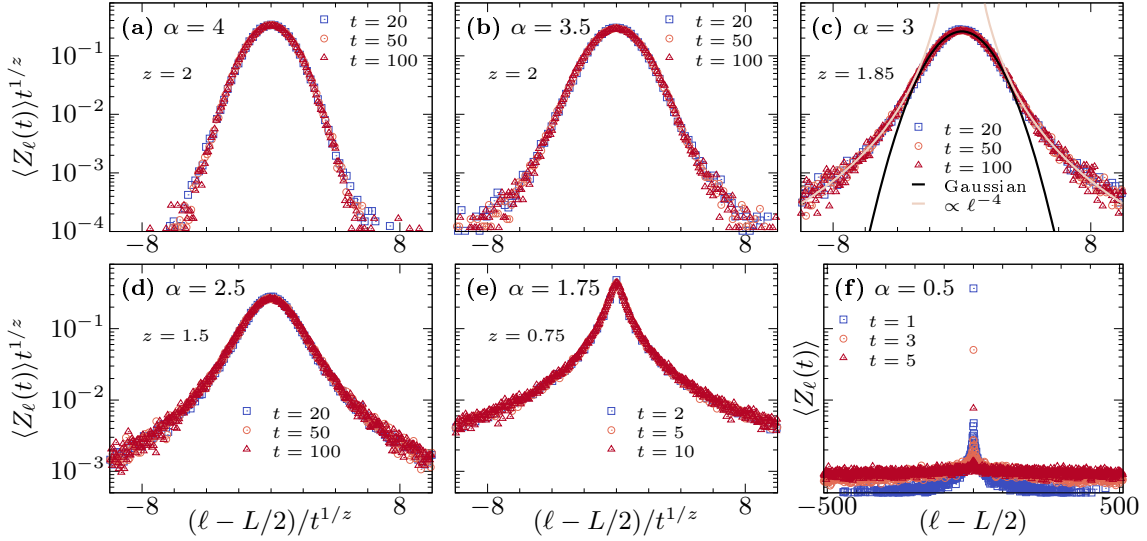


FIG. S1. [(a)-(e)] Rescaled density profile $\langle Z_\ell(t) \rangle t^{1/z}$ versus $(\ell - L/2)/t^{1/z}$ in long-range circuits with different values of α . For $\alpha = 3$, we observe that while the bulk is well described by a Gaussian, the distribution exhibits heavy tails $\propto \ell^{-4}$. (f) $\langle Z_\ell(t) \rangle$ versus $\ell - L/2$ in circuits with $\alpha = 0.5$. The system thermalizes in a few time steps, resulting in a flat distribution.

These update rules for two-site Pauli operators under the action of U(1)-symmetric Clifford gates also allows an understanding of our finding in the context of Figs. 3 (d)-(f). In particular, starting with an isolated X operator, with probability $p = 4 \times 1/8 = 1/2$, a Z operator is created by the first Clifford gate acting on $X \otimes I$. Since this Z operator remains conserved when a gate acts on $Z \otimes I$ [cf. Eq. (S13)], and since the initial operator string contains many I operators, it is highly probable that more Z operators are created due to Eq. (S15) and these Z operators then dominate the spreading of the light cone.

Additional data on hydrodynamics and operator spreading in long-range 1d Clifford circuits

Transport properties

In addition to the data presented in Fig. 2 in the main text, we provide further numerical results on transport in long-range Clifford circuits in Fig. S1. We emphasize that this data can be understood as resulting from the time evolution of an initial state of the form $|\psi(0)\rangle = |\rightarrow\rangle^{\otimes L/2-1} |\uparrow\rangle |\rightarrow\rangle^{\otimes L/2}$. However, due to the particular nature of U(1)-symmetric Clifford gates, i.e., the fact that the stabilizer $\mathcal{O}_i = Z_{L/2}$ will remain of length one throughout the entire circuit, it is in fact not necessary to study $|\psi(t)\rangle$, but just to keep track of the random walk $\mathcal{U}Z_\ell\mathcal{U}^\dagger$ of the isolated Z operator. Averaging over many random circuit realizations yields the expectation value $\langle Z_\ell(t) \rangle$.

In Fig. S1 (a)-(e), the rescaled expectation value $\langle Z_\ell(t) \rangle t^{1/z}$ is plotted versus $(\ell - L/2)/t^{1/z}$ for fixed times t and different values of α . Generally, we find a convincing agreement with the theoretical Lévy-flight prediction [Eq. (2) in main text]. In particular, we observe approximate Gaussian profiles for $\alpha > 3$ that collapse for the diffusive value $z = 2$. Moreover, for $1 < \alpha < 3$, the profile becomes non-Gaussian with a pronounced peak at $\ell = L/2$ and collapses for $z = \alpha - 1$.

Let us now comment on $\alpha = 3$ [Fig. S1 (c)]. In contrast to the prediction of $z = 2$, we find that the numerically obtained value $z \approx 1.85$ yields a much more convincing data collapse. These discrepancies might be due to finite-size and finite-time effects, which we expect to be most pronounced at the phase boundary. Furthermore, while the bulk of $\langle Z_\ell(t) \rangle$ is well described by a Gaussian, consistent with the emergence of diffusive transport for $\alpha \geq 3$, we observe that $\langle Z_\ell(t) \rangle$ exhibits heavy non-Gaussian tails decaying as $\propto \ell^{-4}$, which are well-known to occur for Lévy flights [S5]. It would be interesting to understand in more detail the potential impact of such tails on the dynamics of entanglement $S(t)$ discussed in Fig. 4. In particular, as shown in Fig. S2 below, the operator spreading quantified by $\rho(\ell, t)$ likewise develops such non-Gaussian tails. Let us note that for larger values of α , such as $\alpha = 5$ considered in Fig. 2 (c) in the main text, the density distribution is well described by a Gaussian without heavy tails (at least within the limitations set by the statistical fluctuations).

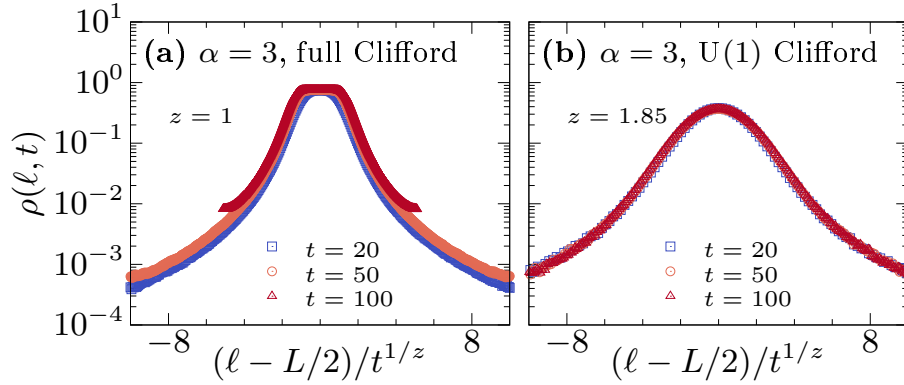


FIG. S2. Circuit-averaged $\rho(\ell, t)$ versus rescaled variable $(\ell - L/2)/t^{1/z}$, obtained analogous to Fig. 3 of the main text. Data is shown for circuits with $L = 1024$ and $\alpha = 3$ for (a) Clifford gates without conservation law and (b) U(1)-symmetric gates.

Eventually, in Fig. S1 (f), we show $\langle Z_\ell(t) \rangle$ obtained in highly non-local circuits with $\alpha = 0.5$. Consistent with the absence of a hydrodynamic tail of $\langle Z_{L/2}(t) \rangle$, cf. Fig. 2 (e), we find that the single Z excitation spreads over the entire system within a few time steps, resulting in a flat distribution.

Operator spreading

To proceed, we also provide additional data on the operator spreading $\mathcal{U}X_{L/2}\mathcal{U}^\dagger$ of an initially isolated X operator, analogous to Fig. 3 of the main text. In Fig. S2 (a) and (b), we focus on $\alpha = 3$ and show cuts of $\rho(\ell, t)$ (see definition in main text) at fixed times for Clifford circuits without conservation law as well as circuits with U(1)-symmetric gates. In the former case [Fig. S2 (a)], we find that $\rho(\ell, t)$ approximately collapses for $z = 1$. Moreover, for the longest time $t = 100$ shown here, $\rho(\ell, t)$ exhibits a flat plateau around $\ell = L/2$ at the saturation value $\rho(\ell, t) = 0.75$, which indicates full scrambling within this area. In the latter case [Fig. S2 (b)], we find that $\rho(\ell, t)$ is similar to the density profiles $\langle Z_\ell(t) \rangle$ in Fig. S1 (c), with a Gaussian shape in the bulk and additional heavy tails. Moreover, as in Fig. S1 (c), we find a data collapse for $z \approx 1.85$. As discussed in the main text, this similarity of $\langle Z_\ell(t) \rangle$ and $\rho(\ell, t)$ is expected in U(1)-symmetric circuits since $\mathcal{O}(t)$ will quickly be dominated by Z operators such that the operator spreading will be impacted by the hydrodynamic behavior of the conserved quantity. Moreover, we note that the value of $z \approx 1.85$ seems consistent with the growth of entanglement discussed in Fig. 4, where we found deviations from the theoretically expected $z = 2$ at $\alpha = 3$. We here leave it to future work to study finite-size and finite-time effects in more details (but see Figs. S5 and S6) and to analyze the potential impacts of the non-Gaussian tails on $S(t)$.

While the operator string $\mathcal{O}(t)$ will quickly be dominated by Z operators in the case of U(1)-symmetric Clifford gates, it is interesting to study how X and Y operators spread within $\mathcal{O}(t)$. Even though their overall weight decays as $\propto t^{-1/z}$ [see inset in Fig. 3 (f) in the main text] their dynamics might differ from the hydrodynamic behavior of the Z operators. To this end, we analyze in Fig. S3 (c) the spreading of X and Y operators in terms of the quantity,

$$\rho_{x,y}(\ell, t) = \sum_{\sigma=x,y} \rho_\sigma(\ell, t) = \sum_{\sigma=x,y} \text{tr}[\mathcal{O}_\ell(t)\Sigma^\sigma]/2, \quad (\text{S16})$$

where, in contrast to $\rho(\ell, t)$, the sum now runs only over X and Y operators. [As already stated in the main text, $\mathcal{O}_\ell(t)$ denotes the local Pauli or identity matrix at the ℓ th position of the operator string and $\Sigma^{\sigma=x,y,z} = \{X, Y, Z\}$. Given the orthogonality of Pauli matrices, we have $\text{tr}(\mathcal{O}_\ell(t)\Sigma^\sigma)/2 = \delta_{\mathcal{O}_\ell(t), \Sigma^\sigma}$.] Focusing on $\alpha = 5$, we find in Fig. S3 (c) that $\rho_{x,y}(\ell, t)$ spreads diffusively and is qualitatively very similar to our results for $\rho(\ell, t)$ in U(1)-symmetric circuits in the main text. This is highlighted by comparing to Fig. S3 (b), where we show $\rho(\ell, t)$ (i.e., including Z operators) for the same system size $L = 128$. Thus, it appears that not only is the overall number of X and Y operators reduced [cf. Fig. 3 (f)], but the spreading of X and Y operators is also affected by the presence of the conservation law. This fact is further emphasized by comparing the results for $\rho_{x,y}(\ell, t)$ in Fig. S3 (c) to the case of full Clifford circuits without conservation law in Fig. S3 (a) (here $\rho(\ell, t)$ and $\rho_{x,y}(\ell, t)$ are equivalent as no operator is favored), where the spreading is ballistic. Let us note that this slow spreading of X and Y operators in U(1)-symmetric Clifford circuits shown in Fig. S3 (c) appears to differ to more generic Haar-random circuits with conservation law, where conserved operators

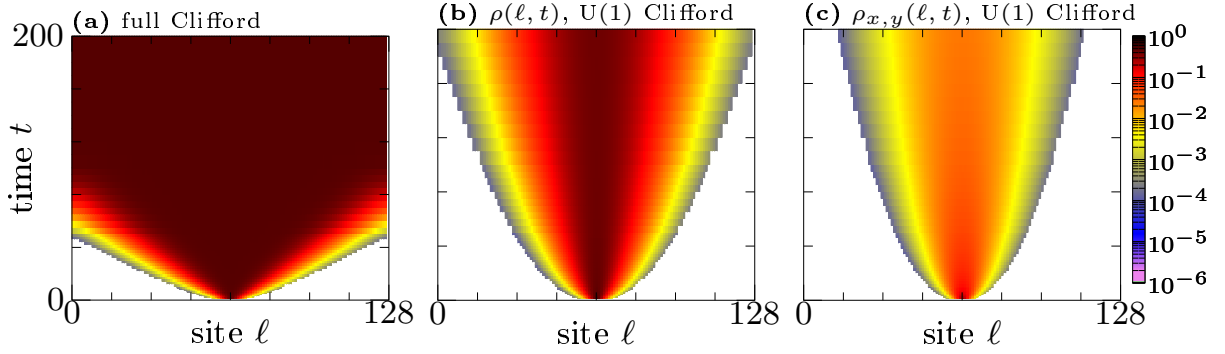


FIG. S3. Operator spreading resulting from $\mathcal{O}(0) = X_{L/2}$ in Clifford circuits with $L = 128$ and $\alpha = 5$. (a) $\rho(\ell, t)$ under full Clifford evolution without conservation law. (b) $\rho(\ell, t)$ in U(1)-symmetric Clifford circuits. Note that data in panels (a) and (b) is analogous to data for $L = 1024$ shown in Figs. 3 (a) and (d) in the main text. (c) $\rho_{x,y}(\ell, t)$ [Eq. (S16)] in U(1)-symmetric circuits.

yield a slow hydrodynamic bulk that lags behind the significantly faster spreading front dominated by nonconserved operators [S3].

Let us now provide some additional analysis regarding the dynamics of the total support $\rho_{\text{tot}}(t)$, already considered in Figs. 3 (c) and (f) in the main text. In particular, in Figs. S4 (a) and (b), we show $\rho_{\text{tot}}(t)$ for different α values in circuits without and with conservation law and two system sizes $L = 1024, 2048$. Comparing the curves for different L , we find that especially for larger values of α , finite-size effects are well-controlled on the time scales shown here. To study the growth of $\rho_{\text{tot}}(t)$ in more detail, Figs. S4 (c) and (d) show its logarithmic derivative. While for large $\alpha = 5$ we recover ballistic behavior ($d \log \rho_{\text{tot}}(t)/d \log t \rightarrow 1$) in the unsymmetric case and diffusive growth ($d \log \rho_{\text{tot}}(t)/d \log t \rightarrow 0.5$) in U(1)-symmetric circuits, we find that the two gate sets behave drastically different at lower α . Specifically, for unsymmetric circuits with $\alpha \lesssim 2$ we are unable to find an extended window with constant $d \log \rho_{\text{tot}}(t)/d \log t$, indicating that $\rho_{\text{tot}}(t)$ is not described by a power law anymore. While this seems consistent with the phase diagram for long-range systems obtained in [S4], where it was argued that the nature of operator spreading changes for $\alpha \leq 2$, we cannot exclude the impact of finite-size/finite-time effects which are clearly more pronounced for smaller α . Interestingly, in contrast to full Clifford evolution, we find that the growth of $\rho_{\text{tot}}(t)$ in U(1)-symmetric circuits appears to be described by a power law for all values of α shown here, with approximately constant $d \log \rho_{\text{tot}}(t)/d \log t$ over an extended time window [Fig. S4 (d)]. Surprisingly, however, we find that the growth of $\rho_{\text{tot}}(t)$ never exceeds ballistic $\propto t$ behavior even for small α , which is somewhat unexpected as transport becomes superballistic for $\alpha < 2$, cf. Fig. 1 (b) in the main text.

In addition to the total support $\rho_{\text{tot}}(t)$ of $\mathcal{O}(t)$, it is instructive to study the left and right endpoints $\rho_L(t)$, $\rho_R(t)$ of the operator string,

$$\rho_L(t) = \min\{\ell \mid \text{tr}[\mathcal{O}_\ell(t)\Sigma^{x,y,z}] \neq 0\}, \quad \rho_R(t) = \max\{\ell \mid \text{tr}[\mathcal{O}_\ell(t)\Sigma^{x,y,z}] \neq 0\}, \quad (\text{S17})$$

which are defined as the smallest and largest lattice site ℓ , for which $\mathcal{O}(t)$ is a non-identity Pauli matrix. For the initial condition $\mathcal{O}(0) = X_{L/2}$, we obviously have $\rho_L(t) = \rho_R(t) = L/2$. For $t > 0$, the difference $|\rho_L(t) - \rho_R(t)|$ is expected to grow. In Figs. S4 (e) and (f), $|\rho_L(t) - \rho_R(t)|/L$ is shown for circuits without and with conservation law and different values of α . While for $\alpha = 5$ we recover ballistic $\propto t$ or diffusive $\propto t^{1/2}$ behavior respectively, the growth of $|\rho_L(t) - \rho_R(t)|$ appears to become more and more similar for smaller α , which is consistent with our observation that entanglement dynamics $S(t)$ becomes essentially unaffected by the conservation law once α is sufficiently small, cf. Fig. 4 in the main text.

Comparing the data of $\rho_{\text{tot}}(t)$ in Figs. S4 (a) and (b) with the results for $|\rho_L(t) - \rho_R(t)|$ in Figs. S4 (e) and (f), we conclude that although the shape of the light cones may become similar for circuits with and without conservation law if α is small, the interior of the light cone behaves notably different. In particular, the comparatively slower growth of $\rho_{\text{tot}}(t)$ in U(1)-symmetric circuits suggests that the operator string $\mathcal{O}(t)$ still contains a larger fraction of identity operators [and as we discussed in Fig. 3 (f), many more Z operators than X and Y], whereas in circuits without conservation law one quickly approaches the equilibrium distribution where X , Y , Z , and identity operators all occur with probability $1/4$.

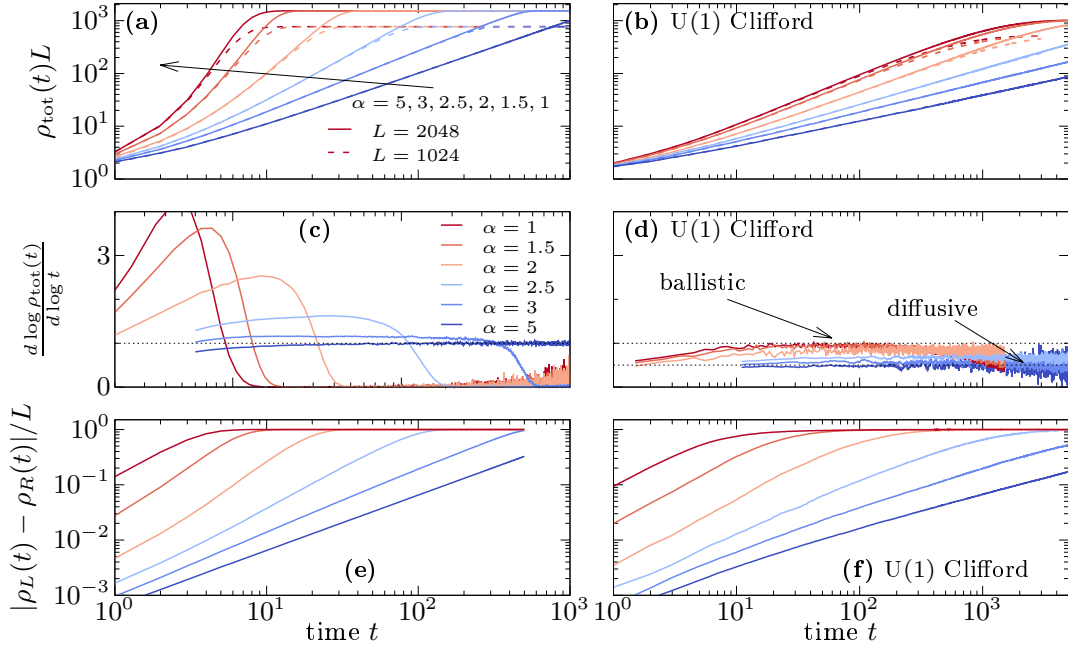


FIG. S4. (a) Total support $\rho_{\text{tot}}(t)L$ of $\mathcal{O}(t)$ for $L = 1024, 2048$ and different values of α (arrow), resulting from isolated operator $\mathcal{O}(0) = X_{L/2}$ under full Clifford evolution without conservation law. Note that data is analogous to Fig. 3 (c) in the main text. (c) Logarithmic derivative $d \log \rho_{\text{tot}}(t)/d \log t$ of the data in panel (a). (e) Normalized difference $|\rho_L(t) - \rho_R(t)|/L$ between left and right endpoint of $\mathcal{O}(t)$, cf. Eq. (S17). Panels (b), (d), and (f) show analogous data, but now for Clifford circuits with U(1)-symmetric gates.

Finite-size scaling of the dynamical exponent z

In this section we explain the procedure we use for estimating the magnitude of finite-size effects in our estimates of the dynamical critical exponent z from the entanglement data. This is necessitated by the fact that we observe fairly significant drifts with system size in our estimates of z , even at the large system sizes $L \sim 10^3$ accessible with Clifford circuits. In passing, we note that it may be the case that Clifford circuits exhibit larger finite-size effects than less structured models, such as Haar-random circuits. It would be interesting to understand better whether the much larger system sizes accessible with Clifford circuits compensate for any larger propensity for significant finite-size effects.

To extract z from the entanglement growth, first for each system size L we calculate the ‘saturation time’ t_{sat} , which for practical purposes we define to be the smallest time at which $S_{L/2}(t)$ is within 1% of its steady-state value. Assuming the entanglement growth is dominated by the asymptotic scaling $S(t) \sim t^{1/z}$ —which empirically is what we observe—and using the fact that the steady-state entanglement is $\mathcal{O}(L)$, the saturation time should scale as $t_{\text{sat}} \sim L^z$. Thus for a given set of system sizes $\{L_i\}$, we can estimate z using a linear fit of $\log t_{\text{sat}}$ vs $\log L$.

To account for finite-size effects, we artificially restrict the dataset we use for this fit to system sizes $L \leq L_{\text{end}}$ for some maximum L_{end} , obtaining a corresponding estimate $z(L_{\text{end}})$. We then vary L_{end} from $L_{\text{end}} = 128$ to the largest system size available, typically $L_{\text{end}} = 1024$ or 2048 depending on the value of α .

Having obtained a range of estimates $\{z(L_{\text{end}})\}$ for different values of L_{end} , we perform an initial fit of these estimates to a power-law, $z(L_{\text{end}}) = b(x_0 + 1/L_{\text{end}})^{-a}$. In principle this initial fit can be used to perform the extrapolation of z as $1/L_{\text{end}} \rightarrow 0$. However, this may give undue weight to this particular power-law fit, since the extrapolated value at 0 can depend somewhat sensitively on the parameters of the fit. To account for this, we perform a form of ‘least squares Monte Carlo’, over a parameter space centered around the parameters obtained from the initial fit. We randomly draw a set of parameters $\mathbf{p} = (a, b, x_0)$ with probability proportional to the inverse square of the least squares cost function $\epsilon(\mathbf{p}) = \sum_i (y_{\mathbf{p}}(x_i) - y_i)^2 / \sigma_i^2$, where $y_{\mathbf{p}}(x_i) = b(x_0 + x_i)^{-a}$, and the data (x_i, y_i, σ_i) are the values of $1/L_{\text{end}}$, the corresponding estimates $z(L_{\text{end}})$, and their errors. For each set of parameters \mathbf{p} we obtain an estimate of the extrapolated value at $1/L_{\text{end}} = 0$. To get our final estimate of z , we draw 10^5 Monte Carlo samples, and take the median extrapolated value. The lower and upper error bars are given by the values of z at which 2.5% and 97.5% respectively of the extrapolated values are below these thresholds.

These extrapolation procedures are shown in Figs. S5 and S6 for U(1)-symmetric and asymmetric Clifford circuits

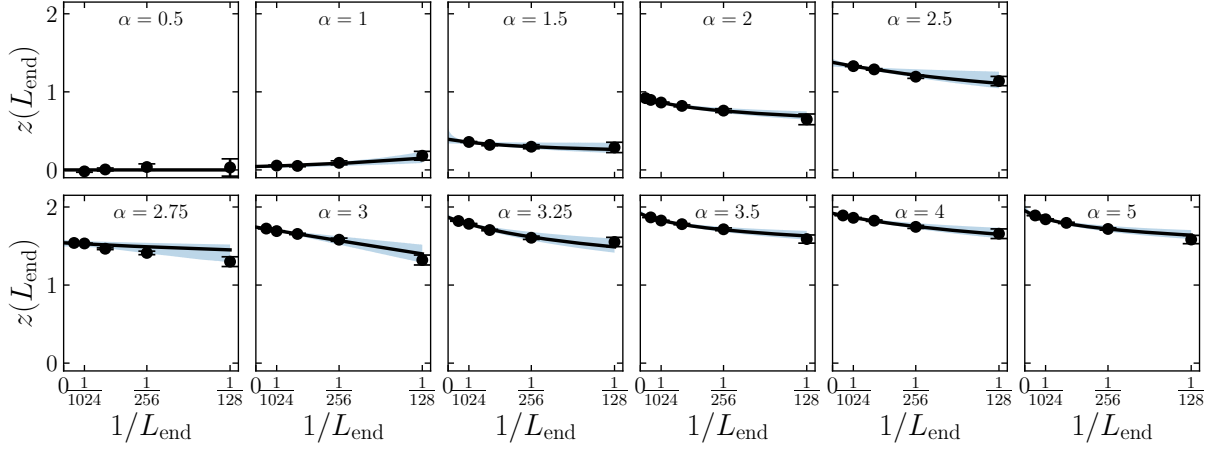


FIG. S5. Extrapolation procedure for the dynamical critical exponent z in U(1)-symmetric Clifford circuits, for different values of α . Data points come from estimates using a linear fit of $\log t_{\text{sat}}$ vs $\log L$, while the black line is the median fit from the ‘least squares Monte Carlo’ procedure described in the main text, and the shaded blue area is the corresponding 95% confidence interval. In most cases the trend as $1/L_{\text{end}} \rightarrow 0$ is for the z estimate to increase, except at $\alpha = 1$, where the estimate decreases towards zero, and $\alpha = 0.5$, where the estimate remains very close to zero.

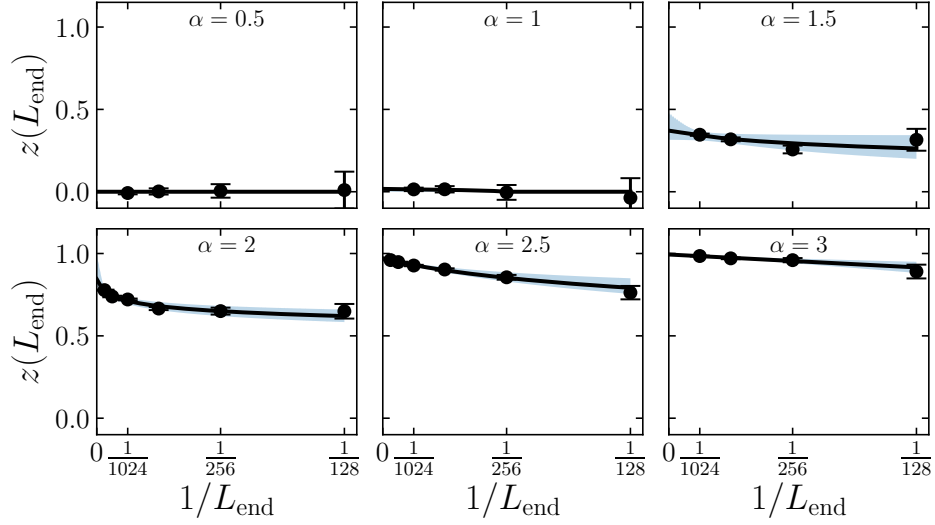


FIG. S6. Extrapolation procedure for the dynamical critical exponent z in asymmetric Clifford circuits, for different values of α . Data points come from estimates using a linear fit of $\log t_{\text{sat}}$ vs $\log L$, while the black line is the median fit from the ‘least squares Monte Carlo’ procedure described in the main text, and the shaded blue area is the corresponding 95% confidence interval.

respectively. In most cases the trend as $1/L_{\text{end}} \rightarrow 0$ is for the z estimate to increase, except for U(1)-symmetric circuits at $\alpha = 1$, where the estimate decreases towards zero, and for the same circuits at $\alpha = 0.5$, where the estimate remains very close to zero. We note that the uncertainty in the estimate seems to be larger around $\alpha \approx 3$, where the transition occurs from short- to long-range behavior. As discussed in the main text, this may be related to the fact that both $\langle Z_\ell(t) \rangle$ and $\rho(\ell, t)$ develop heavy non-Gaussian tails at $\alpha \approx 3$ (see Fig. S1). We defer further investigation of this relationship to future work.

Comparison between long-ranged circuits and circuits with nearest-neighbor gates

For sufficiently large α , the properties of circuits with long-range interactions approach those of strictly local circuits. This fact is demonstrated in Fig. S7, where we compare transport and entanglement growth in long-range circuits

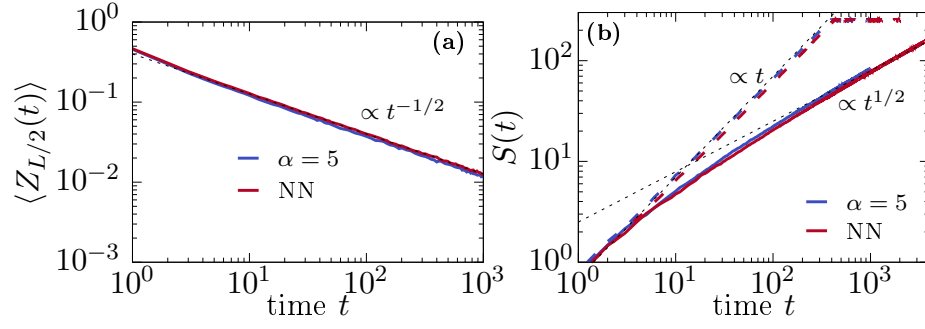


FIG. S7. **(a)** $\langle Z_{L/2}(t) \rangle$ for long-range circuits with $\alpha = 5$ and circuits with nearest-neighbor (NN) gates, obtained analogous to Fig. 2 in the main text. **(b)** Corresponding entanglement growth in circuits with U(1) conservation law (solid curves), resulting from the initial state $|\rightarrow\rangle^{\otimes L}$. As a comparison, we also show $S(t)$ for circuits without conservation law (dashed curves). In all cases, we have $L = 512$ and periodic boundary conditions.

with $\alpha = 5$ and circuits with nearest-neighbor gates. As shown in Fig. S7 (a), the spin excitation $\langle Z_{L/2}(t) \rangle$ decays diffusively $\propto t^{-1/2}$ for both circuit variants and the data for the two different circuits agree very well with each other. Likewise, the entanglement production in long-range circuits with $\alpha = 5$ is essentially equivalent to that in local circuits. In particular, we find that $S(t)$ growth diffusively $\propto t^{1/2}$ at long times for circuits with U(1) conservation law, and linearly $\propto t$ for circuits without charge conservation.

Comparison between random Clifford circuits and Haar-random circuits

Let us briefly compare entanglement dynamics in Clifford circuits to the case of Haar-random circuits. Such a comparison is shown in Fig. S8 (a) for circuits without conservation law and in Fig. S8 (b) for circuits with U(1)-symmetric gates. We here focus on $\alpha = 2$ and $\alpha = 5$ and show data for three different systems sizes $L = 14, 16, 18$ (note that in contrast to Clifford circuits, the simulation of Haar-random circuits is exponentially costly in L). While for Clifford circuits all Rényi entropies are equivalent, we show $S_2(t)$ in the case of Haar-random gates.

On one hand, for the case without conservation law, we find that the entanglement dynamics is very similar for Clifford and Haar-random circuits, which emphasizes the fact that random Clifford circuits form unitary 2-designs and can imitate the properties of more generic types of unitary evolution. On the other hand, in the U(1)-symmetric case, we find that the dynamics of $S(t)$ is again qualitatively similar in Clifford and Haar-random circuits, but $S(t)$ appears to saturate slightly faster towards its steady-state value for Haar-random gates. As already discussed in the context of Eqs. (S8)-(S11), we attribute this difference to the fact that the set of U(1)-symmetric Clifford gates contains a comparatively high percentage of separable gates that generate no entanglement. We expect, however, that this will not change the dynamical critical exponent z , but only affect the coefficient of the $S(t) \propto t^{1/z}$ scaling. In particular, in

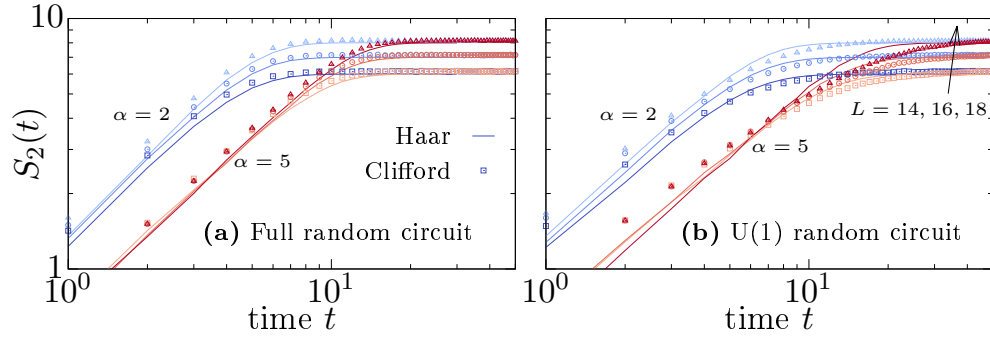


FIG. S8. Entanglement $S(t)$ for $\alpha = 2$ and $\alpha = 5$ in circuits **(a)** without conservation law and **(b)** with U(1)-symmetric gates. We compare the case of random Clifford circuits (symbols) to circuits where the two-site gates are randomly drawn according to the Haar measure (curves). Data is shown for circuits with $L = 14, 16, 18$ and periodic boundaries. While for Clifford circuits all Rényi entropies are equivalent, we show $S_2(t)$ for Haar-random circuits.

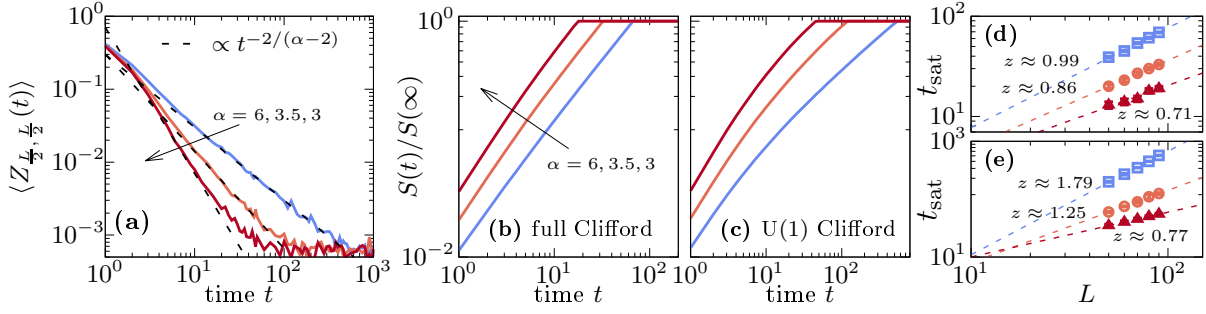


FIG. S9. Transport and entanglement growth in $2d$ lattices. **(a)** $\langle Z_{\frac{L}{2}, \frac{L}{2}}(t) \rangle$ for different α and $L = 40$. Dashed lines indicate power-laws $\propto t^{-d/(\alpha-d)}$. **(b)** $S(t)$ for a half system bipartition under full Clifford evolution with $\alpha = 6, 3.5, 3$ in 90×90 lattice with periodic boundaries. **(c)** Analogous to (b), but now for Clifford circuits with U(1) conservation law. **[(d),(e)]** Saturation time t_{sat} of $S(t)$ versus $L \in [50, 90]$ for full and U(1)-symmetric circuits. The exponent z of the fitted power-law scaling $t_{\text{sat}} \propto L^z$ is indicated next to the data. For $\alpha \lesssim 3$, the scaling in circuits with and without conservation law is found to become similar.

the thermodynamic limit $L \rightarrow \infty$, we expect that the dynamics of $S(t)$ in U(1)-symmetric Clifford circuits at finite times is representative of the dynamics of higher Rényi entropies $S_{n>1}(t)$ in more generic quantum many-body systems.

Two-dimensional circuits

Given the efficient simulability of Clifford circuits, we are able to study transport and entanglement growth also in two-dimensional long-range quantum systems, which would otherwise be challenging even for state-of-the-art numerical techniques. We consider circuits with square geometry and total qubit number $L^2 = L \times L$. Similar to the $1d$ case discussed in the main text, a single time step is defined as the application of L^2 random two-qubit gates of range r , drawn according to the probability distribution $P(r) \propto r^{-\alpha}$. Specifically, for two qubits at positions (x_1, y_1) and (x_2, y_2) , we define r as

$$r = |x_1 - x_2| + |y_1 - y_2|. \quad (\text{S18})$$

Analogous to our analysis in Fig. 2, we study transport by considering the U(1)-symmetric Clifford evolution of an isolated Z operator initially defined at the central site of the $2d$ lattice, $\mathcal{U} Z_{\frac{L}{2}, \frac{L}{2}} \mathcal{U}^\dagger$. Crucially, the picture of long-range random walks of the single Z operator discussed in the main text generalizes directly to higher-dimensional lattices, i.e., for a single circuit realization the operator will always remain of length one. For the circuit-averaged dynamics of the Z excitation, the U(1) conservation law then leads to a power-law decay, $\langle Z_{\frac{L}{2}, \frac{L}{2}}(t) \rangle \propto t^{-d/z}$, which reflects the different α -dependent hydrodynamic regimes. In particular, based on the prediction from Lévy flights (see [S5]), we expect diffusion ($z = 2$) for $\alpha \geq d + 2$, while $z = \alpha - d$ for $d < \alpha \leq d + 2$, and a breakdown of hydrodynamics for $\alpha < d$. For $d = 2$, this yields

$$z = \begin{cases} 2, & \alpha \geq 4 \\ \alpha - 2, & 2 < \alpha \leq 4 \end{cases}. \quad (\text{S19})$$

Let us emphasize again that for Hamiltonian systems with coupling constant $J \propto r^{-\alpha'}$, these bounds have to be rescaled according to $\alpha = 2\alpha'$ [S4, S5]. Focusing on $\alpha = 6, 3.5, 3$, Fig. S9 (a) unveils a convincing agreement of our numerics with Eq. (S19), where we consider $\langle Z_{\frac{L}{2}, \frac{L}{2}}(t) \rangle$ in circuits of size 40×40 . Note that for smaller α , the analysis becomes more difficult due to finite-size effects.

We now turn to entanglement dynamics in $2d$ circuits. To this end, we consider circuits with periodic boundary conditions and calculate $S(t)$ for a half-system bipartition. In Figs. S9 (b) and (c), we show $S(t)$ for circuits without conservation law as well as for U(1)-symmetric Clifford circuits, where we again focus on $\alpha = 6, 3.5, 3$. As expected, the growth of $S(t)$ is notably slower in U(1)-symmetric circuits due to the constraint imposed by the conservation law. However, as was already discussed in Ref. [S6], we find that it is actually rather difficult to observe the conjectured asymptotic scaling $S(t) \propto t^{1/z}$. Therefore, we here proceed analogous to our analysis in the context of Fig. 4 and extract the saturation time t_{sat} of $S(t)$ for circuit sizes ranging from 50×50 to 90×90 , see Figs. S9 (d) and (e). [See labels next to the data in Figs. S9 (d) and (e) for the obtained values of z .] In particular, for circuits without

conservation law and $\alpha = 6$, we recover the expected linear growth of $S(t)$ with $z \approx 1$. In contrast, for $U(1)$ -symmetric circuits, we find a substantially larger value $z \approx 1.79$, which is however smaller than the conjectured value $z = 2$. The deviation from the diffusive value may be due to finite-size effects [S6], and we note that similar deviations also occurred in $1d$ circuits discussed in Fig. 4. Interestingly, for $\alpha = 3$, we find that the scaling of t_{sat} becomes again rather similar for both circuit variants. Analogous to our discussion of $1d$ circuits in the main text, this finding can be understood due to the fact that transport becomes ballistic or superballistic for $\alpha \leq 3$ in $2d$, such that the presence of the hydrodynamic mode becomes less and less relevant.

* j.richter@ucl.ac.uk

- [S1] A. D. Córcoles, J. M. Gambetta, J. M. Chow, J. A. Smolin, M. Ware, J. D. Strand, B. L. T. Plourde, and M. Steffen, Phys. Rev. A **87**, 030301(R) (2013).
- [S2] R. Koenig and J. A. Smolin, J. Math. Phys. **55**, 122202 (2014).
- [S3] V. Khemani, A. Vishwanath, and D. A. Huse, Phys. Rev. X **8**, 031057 (2018).
- [S4] T. Zhou, S. Xu, X. Chen, A. Guo, and B. Swingle, Phys. Rev. Lett. **124**, 180601 (2020).
- [S5] A. Schuckert, I. Lovas, and M. Knap, Phys. Rev. B **101**, 020416 (2020).
- [S6] M. Žnidarič, Commun. Phys. **3**, 100 (2020).